Computer Methods and Programs in Biomedicine 190 (2020) 105378

Contents lists available at ScienceDirect

Computer Methods and Programs in Biomedicine

journal homepage: www.elsevier.com/locate/cmpb

Automatic gauze tracking in laparoscopic surgery using image texture analysis

Eusebio de la Fuente López*, Álvaro Muñoz García, Lidia Santos del Blanco, Juan Carlos Fraile Marinero, Javier Pérez Turiel

ITAP (Instituto de Tecnologías Avanzadas de la Producción), University of Valladolid, School of Industrial Engineering, Paseo del Cauce, 59, 47011 Valladolid, Spain

ARTICLE INFO

Article history:
Received 3 August 2019
Revised 17 January 2020
Accepted 30 January 2020

Keywords:
Computer-aided-surgery
Gossypiboma
Image Texture Analysis
Local Binary Patterns (LBP)
Convolutional Neural Networks
Minimally Invasive Surgery

ABSTRACT

Background and Objective: Inadvertent retained surgical gauzes are an infrequent medical error but can have devastating consequences in the patient health and in the surgeon professional reputation. This problem seems easily preventable implementing standardized protocols for counting but due to human errors it still persists in surgery. The omnipresence of gauzes, their small size, and their similar appearance with tissues when they are soaked in blood make this error eradication really complex. In order to reduce the risk of accidental retention of surgical sponges in laparoscopy operations, in this paper we present an image processing system that tracks the gauzes on the video captured by the endoscope.

Methods: The proposed image processing application detects the presence of gauzes in the video images using texture analysis techniques. The process starts dividing the video frames into square blocks and each of these blocks is analyzed to determine whether it is similar to the gauze pattern. The video processing algorithm has been tested in a laparoscopic simulator under different conditions: with clean, slightly stained and soaked in blood gauzes as well as against different biological background tissues. Several methods, including different Local Binary Patterns (LBP) techniques and a convolutional neural network (CNN), have been analyzed in order to achieve a reliable detection in real time.

Results: The proposed LBP algorithm classifies the individual blocks in the image with 98% precision and 94% sensitivity which is sufficient to make a robust detection of any gauze that appears in the endoscopic video even if it is stained or soaked in blood. The results provided by the CNN are superior with 100% precision and 97% sensitivity, but due to the high computational demand, real-time video processing is not attainable in this case with standard hardware.

Conclusions: The algorithm presented in this paper is a valuable tool to avoid the retention of surgical gauzes not only because of its reliability but also because it processes the video transparently and unattended, without the need for additional manipulation of special equipment in the operating room.

1. Introduction

Inadvertent retained surgical gauzes are a medical error that occurs rarely but can cause very serious complications in the patient due to the formation of *gossypibomas* (from the Latin *Gossypium*, cotton and the suffix *-boma*: tumor). Gossypibomas are difficult to diagnose and cause infections, sepsis, intestinal obstructions and visceral perforations [32], even leading to death in 2% of cases [8]. The increasing number of recent reports in the literature implies that gossypibomas still remain as an important problem to be solved.

There is a risk of accidental retention of surgical objects in all types of surgery. However, the data show that abdominal surgery is where this malpractice occurs most often (1 in every 1000 to 1500 operations) [8]. Among the objects accidentally retained, surgical gauze is the most frequent item [4,18,34,36], with an incidence of approximately one retained gauze per 2000 operations. Surgical gauzes are easily masked between the tissues and organs when soaked in blood and other fluids, especially when operating in the abdominal cavity. Unfortunately, it is precisely the gauzes

* Corresponding author.
E-mail addresses: efuente@eii.uva.es (E. de la Fuente López), alvaro.munoz.garcia@alumnos.uva.es (Á. Muñoz García), lidia.santos@uva.es (L. Santos del Blanco), jcfraile@eii.uva.es (J.C. Fraile Marinero), turiel@eii.uva.es (J. Pérez Turiel).

https://doi.org/10.1016/j.cmpb.2020.105378

that cause the more severe reaction in the organism among all the retained foreign objects.

There are many possible causes for this type of error. These include the inadequate organization in the operating room, the pressure in emergency operations, distractions that occur especially in very long operations and changes in procedure [4,8,12,36].

Standard protocols to prevent the retention of surgical items are customary in all hospitals. The procedure usually consists of two nurses counting all surgical instruments and articles used in the operation at the beginning and at the end of it [8]. This method, which may seem to be unquestionably reliable, is not completely trustworthy due to human errors [35]. Some studies show that 88% of retained foreign objects have occurred after the count was reported as correct [8]. Many authors, therefore, have justified the research aimed at developing new technologies to reliably monitor gauze and eradicate gossypibomas [4,31,35].

When gauze accounting is not balanced, the missing gauze must be located taking radiography and then exposing the patient to X-radiation and longer-term anesthesia. Although the bandages include some kind of opaque X-ray marking to allow detection on X-rays, they are not infallible either. It is estimated that the rate of intraoperative detection on simple X-rays is only 67% [4].

Fortunately, new technologies are being introduced in recent years to avoid relying solely on manual counting. A first improvement is the use of barcode surgical sponges [9]. The barcode is integrated into each gauze and is different in each of them. Using a handheld reader, the control is carried out by reading the code of each gauze that enters and exits the patient's body. In the event of a failure at the end of the procedure, it can even be established which gauze has disappeared. The reader is able to record codes even on blood-stained sponges. However, the use of this system introduces new technical difficulties that slow down the counting process by approximately 3 minutes.

Some operating theatres have experimented with more sophisticated devices than barcodes readers such as radiofrequency systems. This technology is capable of reading RFID tags with a unique identification number that have been attached to the surgical gauze. The presence of a forgotten gauze can be detected by passing a portable handheld antenna in front of the surgical field when the operation is finished [35]. Another system presented in [15] to minimize the intervention of health personnel in the gauze count, incorporates three antennas: one for the initial check-up, another installed in the wastebasket and another fixed antenna that scans the patient. The authors claim that the sensitivity and precision of this type of device is 100% and allows a great saving of operating time, 28 minutes in each surgical procedure. However, a recent study [36] where 319 retained surgical sponges where considered reports 5 cases where, although sponge detection technology was noted to be available in the setting, it was not used. It is crucial not only that the gauze detection device is reliable, but also that this is convenient and easy to operate.

Another system for gauze detection is presented in [7]. In this case it is an image processing algorithm that includes a LBP descriptor with two different patterns to deal with illumination changes. The application only reaches a sensitivity of 42.95% and the authors recognize that their technique is too intensive to be run in a real-time detection system.

In this paper, we propose the tracking of surgical gauze by simply processing the video signal from the endoscope. The gauze detection is carried out in real time and without the need to incorporate any additional equipment or adding any type of marker to the gauze. The advantage is that healthcare personnel do not have to operate new equipment such as barcode readers or RFID antennas to track the gauze. The tracking is done in a transparent and totally unattended manner on the video, that is continuously acquired for the visualization of the scene, without requiring additional attention from the surgeon or his assistants.

The application aims to account for the surgical gauzes inside the patient's body using basically the video images from the endoscope. Each incoming gauze is detected by the image processing program that tracks it while it is present within the visual field of the endoscope. If the gauze disappears when is completely immersed in blood or behind any of the patient's organs or tissues, this fact causes the activation of a warning icon at the bottom of the monitor. A mark is also set at that time on the slider of the video being recorded. However, if the loss of the gauze in the image is due to its extraction by the surgeon for disposal, a subsequent activation of an external sensor installed in the wastebasket will cancel the alarm just triggered.

It is necessary to emphasize that this application does not exempt the health personnel from counting. Nevertheless, the activation of the alarm when the automatic system reveals any inconsistency will lead them to be especially cautious. If gauze accounting is effectively not balanced, the application can also be of great help in speeding up the location of lost surgical sponges using the disappearance marks on the video.

The future incorporation of some optical technique for 3D reconstruction in computer-assisted laparoscopic surgery [22], such as Simultaneous Localization and Mapping (SLAM) [5], will make it possible to obtain the position of the gauze when it disappears, without using additional devices. This will make the gauze recovery process faster, more reliable and even suitable to be conducted by a robotic assistant [19].

The rest of the paper is organized as follows. Next section presents the methodology. It introduces a review of the texture analysis technique LBP (*Local Binary Patterns*) and several variants that have been analyzed for the detection of surgical gauzes including also a CNN approach. Section 3 gives a summary of experimentation and Section 4 discusses the results obtained with the different approaches on clean, stained and blood-soaked gauzes. Finally, the conclusions of the work are presented.

2. Methodology

Our application for the detection of gauze is based on the processing of video from the endoscope. Each frame of the video is analyzed looking for areas that present a texture similar to that of the gauze. Texture is a very popular feature in image processing, especially in the medical field, where a multitude of approaches have been used. One of the most powerful and computationally efficient technique for texture analysis is Local Binary Patterns (LBP) [25].

2.1. Local binary patterns

The LBP operator assigns a value to each pixel of the image obtained by comparing the gray level of the pixel with its eight neighbors. If the neighbor's value is greater than or equal to that of the pixel, then a 1 is set in the pattern or a 0 otherwise (see Fig. 1a). The binary pattern generated is transformed into a decimal value that is assigned to the central pixel. The histogram of the resulting image is used as a texture descriptor of the image [21].

The LBP can be extended to deal with circular neighborhoods of different sizes [26] (see Fig. 1b). The notation *(P,R)* specifies a neighbourhood with P evenly sampled points on a circle of radius of R. Then, if the grey level of an arbitrary pixel (x_c,y_c) is g_c and g_p is the grey value of the P sampled points in a circular neighbor-

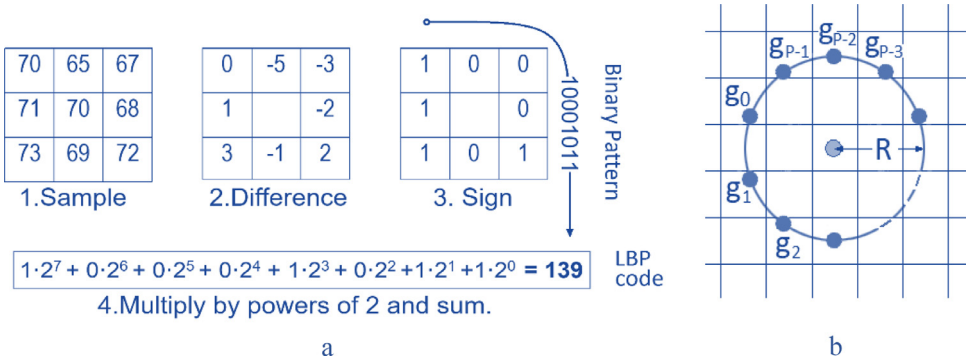

Fig. 1. (a) Example of LBP computing at a pixel. b) Different neighborhoods can be considered in LBP varying the radius R and the number P of evenly spaced neighbors on the circumference of radius *R*.

hood of radius R around point (x_c,y_c):

$$LBP_{P,R}(x_c, y_c) = \sum_{p=0}^{P-1} s(g_p - g_c)2^p \quad (1)$$

where $s(g_p - g_c)$ denotes de sign of the difference, being $s(g_p - g_c) = 1$ if the difference is positive or null and 0 if not.

An invariant rotation version of the LBP is presented in [28], which is especially useful for our application where the texture of the gauze can appear at any angle. The rotation invariant version of the LBP maps all cyclic permutations of a binary LBP code onto the same rotation-invariant pattern, decreasing the number of codes considerably.

The number of codes can be reduced even more because many of the binary patterns appear only rarely in the images. Mäenpää et al. [20] presented a new version of LPB, called uniform LBP, which considered only those patterns that are frequently found in texture images and that are characterized by two transitions at most in the bits of their binary code. The reduction in the number of codes, using only *P+1* uniform patterns, provides a statistical analysis more stable.

Since the presentation of these first LBP operators, numerous variants have been suggested for the classification of textures. The following are only the most appropriate approaches to our application. An exhaustive review of local binary features for texture classification can be found in [16].

Heikkila et al [14] introduced the centre-symmetric local binary pattern (CS-LBP) where, instead of comparing each pixel in the neighbourhood with the central pixel, they compare centre symmetric pairs of pixels thus generating a much shorter 16 features histogram. Later, in order to improve the noise robustness of the operator LBP, Tan [38] proposed the Local Ternary Pattern (LTP). As the name suggests, the neighbouring pixels are encoded with three values: 1 if the grey level difference with the central pixel is above a pre-set threshold, 0 if the absolute value of this difference is below the threshold and -1 if it is the central pixel that exceeds the neighbour's grey level by at least the threshold value.

2.2. Contrast and texture patterns

The LBP methods presented in the previous section show good rotation robustness and are even resistant to slight variations in scene lighting. However, under real conditions, the texture of the gauze can change considerably depending on the distance to the endoscope, the presence of folds or if it is soaked in blood. In addition to local patterns, some form of contrast analysis of the image regions must be included to address this highly variable pattern of the gauze (Fig. 2).

Texture can be understood as a two-dimensional feature characterized by two orthogonal properties: pattern, which is the spatial structure, and contrast, which is the strength of that pattern. Pat-

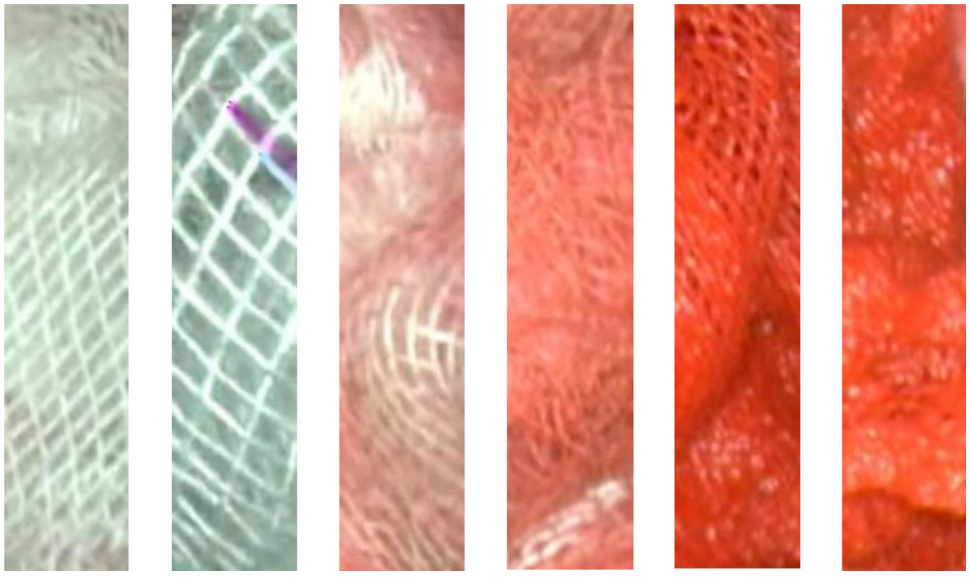

Fig. 2. The texture of the gauze is very changeable depending on the distance to the endoscope, the presence of folds or if it is soaked in blood or other fluids.

tern information is independent of the gray level but contrast is not. These two features complement each other in a very practical way.

The contrast can be measured in a circular neighborhood through variance [26]:

$$VAR_{P,R}\ (x_c, y_c) = \frac{1}{P}\sum_{p=0}^{P-1}(g_p - \mu)^2 \quad (2)$$

where μ is the neighborhood average calculated as follows:

$$\mu = \frac{1}{P}\sum_{p=0}^{P-1} g_p \quad (3)$$

In our previous work [23], several implementations of the gauze detection algorithm using the variance were analyzed. The experiments showed that incorporating local contrast into texture analysis improved both precision and sensitivity of the detection, specially in the case of soaked gauzes.

As $VAR_{P,R}$ has continuous values, it is necessary to quantize it. The distribution of the variance can be calculated on all the model images and, in order to achieve the best resolution in quantization, then compute the threshold values that partition the distribution in *N=16* intervals with equal number of entries [26]. These values will be subsequently used to quantify the variance of the test images.

The variance can be combined into the LBP histogram by using it as weights for LBP. This approach, named LBP variance (LBPV), was introduced by [10] and allow to simplify the computation of a joint LBP and variance distribution. However, in next section we will see that this technique does not provide as satisfactory results as if the LBP and contrast analysis are carried out separately and then combined by a logical OR. We have called this operator LBP|VAR and it reveals that the inclusion of variance information must be adapted to the specific task [33].

Another approach that incorporates information on contrast was presented by Guo et al [11]. In its Complete LBP (CLBP) model, in addition to using the original LBP, they introduce two new operators: CLBP_M, which measures the variance of the magnitude and CLBP_C, which establishes the difference of the central pixel with respect to the average grey level of the entire image. By combining the histograms provided by these three operators, they achieve a significant improvement in texture classification. Based on the CLBP model, Zhao et al [39] suggested a new variant for rotation invariant classification, the Complete Local Binary Count (CLBC), an algorithm that discard the structural information of the CLBP operator. CLBC counts the number of values 1 in the neighbouring binary sets instead of encoding them. CLBP and CLBC operators are analysed for gauze detection in Section 3.

2.3. Dissimilarity measure

In order to find the areas in the image that show a texture similar to that of a gauze, the image will be divided in square blocks of the same size (Fig. 5) and each block will be analyzed individually. Comparing the similarity between the distribution histograms of the model with those of the block, it will be determined if a gauze is present in that block or not.

In this paper, we utilized the chi-square distance to quantify the dissimilarity between two normalized histograms:

$$D(B, M) = \sum_{i=1}^{n}\frac{(B_i - M_i)^2}{(B_i + M_i)} \quad (4)$$

where n is the number of bins, *Mi* is a value of a bin in the model histogram and *Bi* is the value of the same bin in the block histogram.

Fig. 3. Experimental setup. In this image a video with of a clean gauze is being acquired with the Storz Telecam endoscope inside the laparoscopic simulator.

In case of LBP|VAR algorithm, two similarity measures are therefore established between the block and the model. The first one corresponds to the comparison of the LBP histograms and the second one to the variance histograms. The operator LBP|VAR that categorizes a block as gauze when either the LBP histogram or the VAR histogram is sufficiently similar to that of the model has proved to be an effective strategy to classify a block.

3. Material and experimentation

The 720 × 576 video images used in this study were obtained with a STORZ TELECAM [37] One-Chip Camera Head 20212030, color system PAL with integrated focal Zoom Lens, f = 25 – 50 mm (2x), with an image sensor of ½" CCD and 752 (H) x 582 (V) pixels per chip (PAL) equipped with Hopkins telescope 0°, 10 mm, 31 cm.

The test images used in experimentation do not come from laparoscopic surgery operations on real patients. The scenes have been generated in a laparoscopic simulator using animal internal organs in order to recreate scenarios similar to those that appear in real operations (Fig. 3).

This experimental scenario has allowed us to test the algorithm under the different circumstances in which surgical gauzes can appear in this type of operations: clean, slightly stained or soaked in blood or other internal fluids as well as against different biological background tissues.

There are several strategies and parameters that influence the detection results: the potential use of color information, the size of the blocks into which the image is divided, the number of neighbors in the operators, the neighborhood radius and last but not least, the performance of the different LBP approaches in gauze detection. The following subsections present an analysis of the impact of these strategies and parameters on the detection results.

Table 1
Dimensionality and AUC-ROC for different colour methods. Homologous grey level variants clearly outperform the colour methods in the detection of surgical gauzes.

Abbreviation	Variant	No. of Features	AUC ROC
LBP	**Local Binary Patterns Grey scale [25]**	**256**	**0.940**
LBP-RGB	Independent colour components. RGB colour space [2]	768	0.861
LBP-HSV	Independent colour components. HSV colour space	768	0.636
LBP-Lab	Independent colour components. Lab colour space	768	0.495
LBP-YCbCr	Independent colour components. YCbCr colour space	768	0.617
LBPriu	**Rotation invariant and uniform in grey scale [20]**	**10**	**0.957**
LBPriu-RGB	Indep. Colour comp. Rotation invar. and uniform. RGB space	30	0.874
LBPriu-HSV	Indep. Colour comp. Rotation invar. and uniform. HSV space	30	0.699
LBPriu-Lab	Indep. Colour comp. Rotation invar. and uniform. Lab space	30	0.761
LBPriu-YCbCr	Indep. Colour comp. Rotation invar. and uniform. YCbCr space	30	0.760
OCLBP-RGB	Opponent colour LBP. RGB colour space [30]	1.536	0.617
OCLBP –HSV	Opponent colour LBP. HSV colour space	1.536	0.657
OCLBP –Lab	Opponent colour LBP. Lab colour space	1.536	0.651
OCLBP -YCbCr	Opponent colour LBP. YCbCr colour space	1.536	0.694

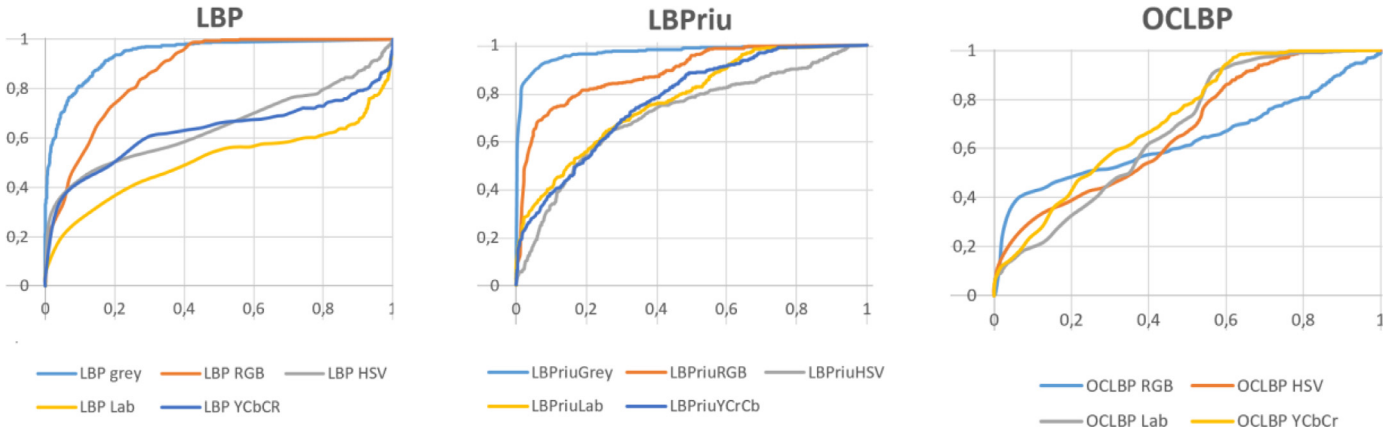

Fig. 4. ROC curves for the LBP, rotation invariant uniform (LBPriu) and opponent colour (OCLBP) variants.

3.1. Color information

Some experiments evaluating the LBP texture features using colour have been conducted. Colour features have been computed considering not only each colour component of the images independently but also tested using the Opponent Colour LBP model (OCLBP) [30]. The first approach generates the LBP histogram concatenating the histogram from each colour components while the second provides the spatial distribution between the different colour components representing the colour texture from 6 LBP histograms. Both experiments have been carried out using different spaces (RGB, YCbCr, HSV and Lab) trying to find the representation the most suited for our application.

We have computed the area under the curve (AUC) of receiver operating characteristics (ROC) curve to compare the classification performance of the different colour models with the grey level ones. AUC measures the quality of model predictions, regardless of which classification threshold is chosen. The higher the AUC, the better the model is at distinguishing between gauze and background.

The results, shown in Table 1 and Fig. 4, reveal that colour models perform visibly below the grey levels models. These models, certainly powerful when discriminating regions with stable colour textures, have not been shown to be advantageous in the detection for two reasons. Firstly, due to the unpredictable colour appearance of gauzes; although initially these items are perfectly white, they adopt very dissimilar tonalities depending on the fluid in which they are impregnated and the amount of liquid they absorb. The second reason is due to the unstable illumination inside the patient body. Colour texture operators in steady illumination conditions are more powerful than operators based only on grey level, but fail when illumination varies [29].

3.2. Size of image blocks

Fig. 5 displays the results for different block sizes, using a LBP operator with a neighborhood P8-R1. The tests show that very small blocks do not give the best results and significantly increase the number of false positives. This is because the area being analyzed is statistically less stable for smaller regions.

On the other hand, for larger block sizes, the analysis areas are significant, but detection is subject to the fact that the gauze occupy a major part of the block, which is difficult when the block size is increased excessively. In the last image of Fig. 5 the blocks are only partially filled by the texture of the gauze, which causes failures in detection. Eventually, a block size of 100 × 100 pixels has been chosen as a compromise between these two facts.

3.3. Number of neighbors and radius of the neighborhood

Several rotation invariant uniform (*LBPriu*) operators have been implemented using three different neighborhood sizes P (8, 12 and 16) and three different radii R (1,2 and 3). The influence of the number of neighbors and the radius on the detection results is presented in two graphs (Fig. 6). For the analysis of the radius (Fig. 6a), the average precision and sensitivity have been computed using three neighborhoods with different values P (8, 12 and 16) for each of the three radii. Analogously for the analysis of the number of neighbors. These tests were carried out using a block size of 100 × 100 pixels.

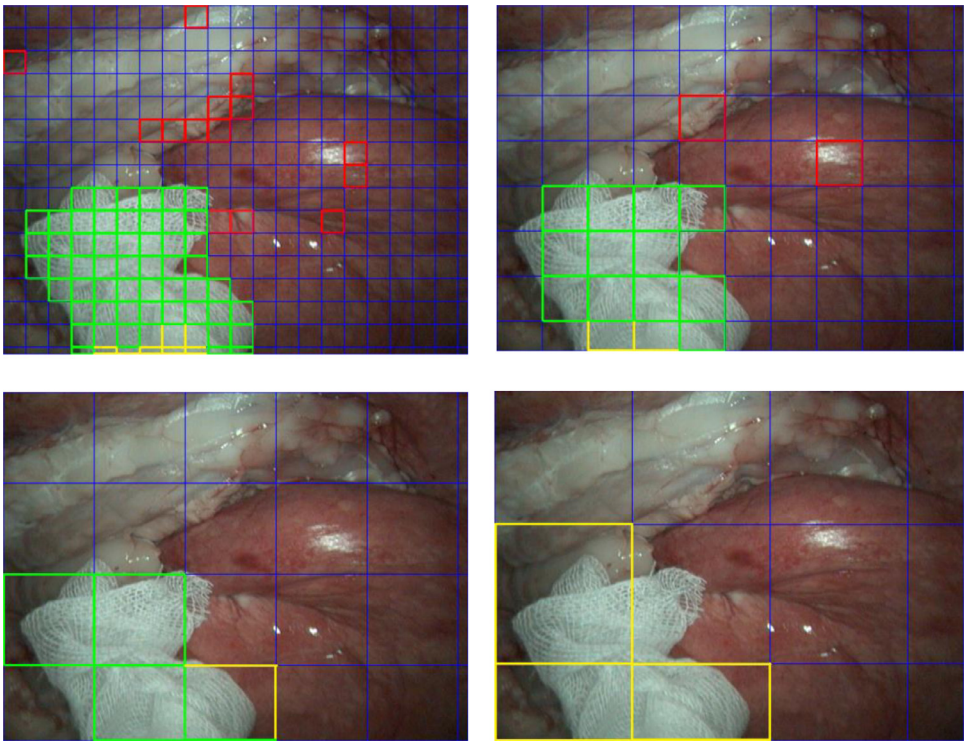

Fig. 5. Influence of block size. Blocks detected correctly as gauze *(true positives)* appear in green, erroneously classified as background *(false negatives)* in yellow and, wrongly detected as gauze *(false positives)* in red.

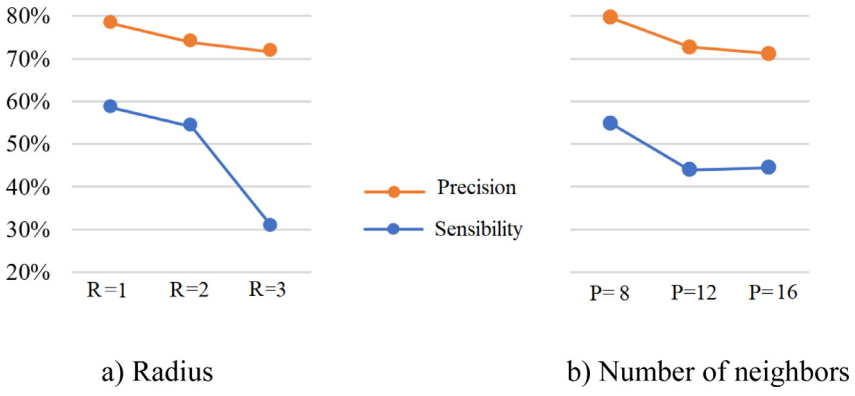

Fig. 6. Influence of radius and number of neighbors in precision and sensitivity.

Fig. 6a shows that as the radius increases, both precision and sensitivity decrease. The effect is more noticeable in sensitivity. A similar trend can be perceived when the number of neighbors varies (Fig. 6b). As the number of neighbors increases, precision and sensitivity decrease. In the latter case, although the sensitivity increases slightly when we change from 12 to 16 neighbors, the difference is minimal and a descending trend can be assumed. Thus the experiments allow to conclude that the highest values of precision and sensitivity are achieved with a unit radius neighborhood and 8 neighbors.

3.4. LBP variants

Several LBP variants have been programmed (see Table 2) and the performance of each method has been evaluated by quantifying the AUC-ROC. For this analysis, we used blocks 100 × 100 extracted from images, 4891 blocks classified as background and 1782 blocks of gauze in different circumstances (clean, stained and soaked) (link to dataset) . 75% of these blocks have been used to obtain the pattern histogram and the remaining 25% has been reserved for the test with which we have obtained the ROC curves.

The variants with the best performance are those that somehow incorporate information about contrast. The CLBC proposed by [39], although it contains this type of information, did not provide good results, probably because the structural information, that seems to be important for the classification, is discarded in this model.

The multi-resolution approach [26] using 8 neighbours and two different radii, R=1 and R=2, doubles the computational cost and does not offer any improvement with respect to the unit radius approach. The most interesting variants after this study are LBP|VAR and CLBP (see Table 2). Next section shows that both provide satisfactory results in gauze detection with a low computational load.

3.5. Convolutional neural network approach

In recent years, deep Convolutional Neural Networks (CNN) have provided spectacular results in many fields of machine vision including texture classification. They have also shown excel-

Table 2
Dimensionality and AUC-ROC for the different LBP grey level methods.

Abbreviation	Variant	No. of Features	AUC ROC
LBP	Local Binary Patterns in grey scale [25]	256	0.940
LBPriu	Rotation invariant and uniform in grey scale [20]	10	0.957
LBP|VAR8,1+8,2	Multiresolution LBPriu and variance (8,1) and (8,2) [26]	20	0.957
VAR	Variance distribution [26]	16	0.954
LBP|VAR	Local Binary Pattern or Variance [23]	26	**0.965**
LBPV	Local Binary Pattern Variance [10]	10	0.945
CS-LBP	Center-Symmetric Local Binary Patterns [14]	16	0.921
LTP	Local Ternary Pattern [38]	512	0.943
CLBP	Completed Local Binary Pattern [11]	30	**0.974**
CLBC	Completed Local Binary Count [39]	32	0.941

lent discrimination performance, especially under very changing acquisition conditions where they have proved to be superior to hand-crafted descriptors [1,17].

Among CNN, ResNet models [13] appear as one of the best approaches for texture analysis in realistic conditions [1]. The ResNet50 model presents a good tradeoff between inference time and accuracy among a wide variety of models analyzed in terms of inference time, accuracy and power consumption [3].

In order to contrast the experimental results of our LBP model with a CNN approach, a ResNet50 model has been trained for our gauze detection application using the PyTorch framework. Since the size of our dataset is limited, we have used a pre-trained model to obtain reliable results. In order to enable the current pre-trained model to be able to classify our two classes, background and gauze, the final layer of the model has been changed by the following set of sequential layers. Firstly, it has been connected to a linear layer with 256 outputs that is followed by a ReLU and Dropout layers and finally a 256×2 lineal layer, with the two outputs corresponding to the classes to be identified. The negative loss likelihood function was used to determine the loss and the selected optimizer was the Adam optimizer.

Our dataset (link to dataset) consists of 4891 images of background and 1782 of gauze. We have used, for each class, 1000 images for training, 300 images for validation and the rest for testing, all of them randomly selected. The training process consisted on 25 epochs which has been analyzed in terms of loss and accuracy, choosing the model that offered the highest accuracy ratio and lower loss.

4. Results

Our gauze detection algorithms classify each of the blocks into which the image has been divided as gauze or background. They carry out this task based on the similarity between the image blocks and the gauze model pattern. As this classification is not faultless, among the true positives (tp) and true negatives, there will appear false negatives (fn) and false positives (fp). The precision and sensitivity, also called recall, can be used to quantify the performance of the algorithm:

$$precision = \frac{tp}{tp + fp} \tag{5}$$

$$sensitivity = \frac{tp}{tp + fn} \tag{6}$$

The percentages of precision and sensitivity shown in the following subsections correspond to the average of 110 simulated laparoscopic images that can be divided into three groups: images containing clean or almost clean gauzes (47 images), images with gauzes stained with blood (31 images), images with gauzes totally soaked in blood (28 images) and images where no gauze is present (4 images). (Link to the suite of test images)

Table 3
Precision and sensitivity obtained by the LBPriu and LBP|VAR versions.

	LBPriu		LBP|VAR	
Image content	Precision	Sensitivity	Precision	Sensitivity
Clean gauze	1.00	0.81	1.00	0.88
Stained gauze	0.96	0.72	0.95	0.85
Soaked gauze	0.86	0.53	0.90	0.87
Overall	**0.96**	**0.72**	**0.96**	**0.86**

In order to obtain a ground truth, the blocks in the suite of 110 test images have been manually segmented marking those blocks in which the gauze occupies at least 75% of the block. The comparison of the ground truth segmentation with the results provided by the algorithm permit to stablish the number of true positives, false negatives and false positives and quantify the precision and recall in the classification of individual blocks.

4.1. LBP|VAR operator

To better quantify the performance of the developed algorithm, a first version, only based on the LBPriu operator, was executed without any analysis of variance. The results, broken down according to the content of the images, are presented in Table 3 (More detailed tables can be accessed in the following links: table LBPriu, table LPB|VAR). These results show that the technique based only on LPB is not reliable for the detection of the gauze in this practical application.

LBP have good detection capacity when the texture appears clearly in the image as in the case of clean or slightly stained gauzes. When gauzes are soaked or the image is blurred by the movement of the endoscope, the characteristic texture of the gauze disappears and the algorithm lose its detection capacity. In these situations, where the LBP operator fails due to the loss of the local spatial pattern, the VAR operator complements the recognition. Incorporating variance into the analysis algorithm permits a considerable increase in sensitivity, especially in the cases of soaked gauzes and when images are blurred (Fig. 7).

4.2. Completed LBP (CLBP) operator

The results provided by the completed LBP variant (CLBP) [11] are significantly better than those achieved with the basic LBP operator (Table 4). This is due to the fact that the CLBP algorithm introduces, besides the sign differences between neighbours and central pixel, the magnitude differences of each pattern with the central grey level of the patterns.

The CLBP variant improves the precision and sensitivity of the LBP|VAR algorithm but this one seems more robust to image blurring (Figs. 7b and 8c). Unfortunately, both of them suffer from a lack of detection in saturated image areas.

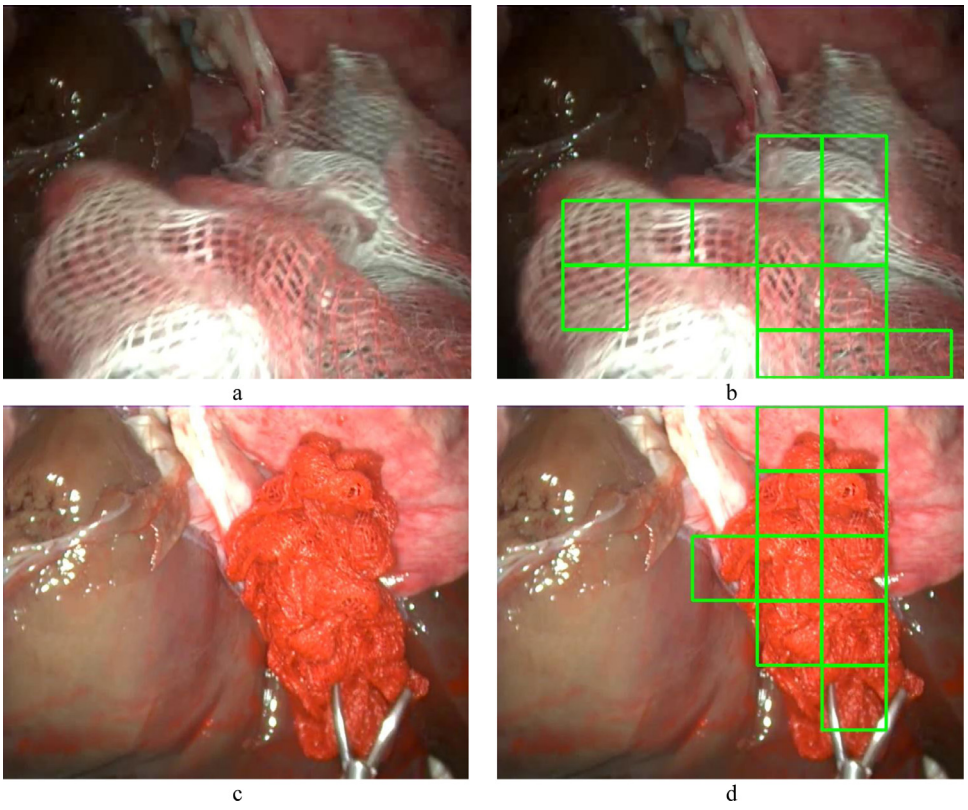

Fig. 7. The LBPriu operator could not detect any block in images *a)* and *c)*. It usually fails in blurred images and in the detection of soaked gauzes due to the loss of the gauze spatial microstructure. *b)* and *d)* Results of LPB|VAR operator in the same images. In these situations, the variance operator is crucial in the gauze recognition task. (The results obtained on all the images can be accessed in the following links: results LBPriu and results LBP|VAR).

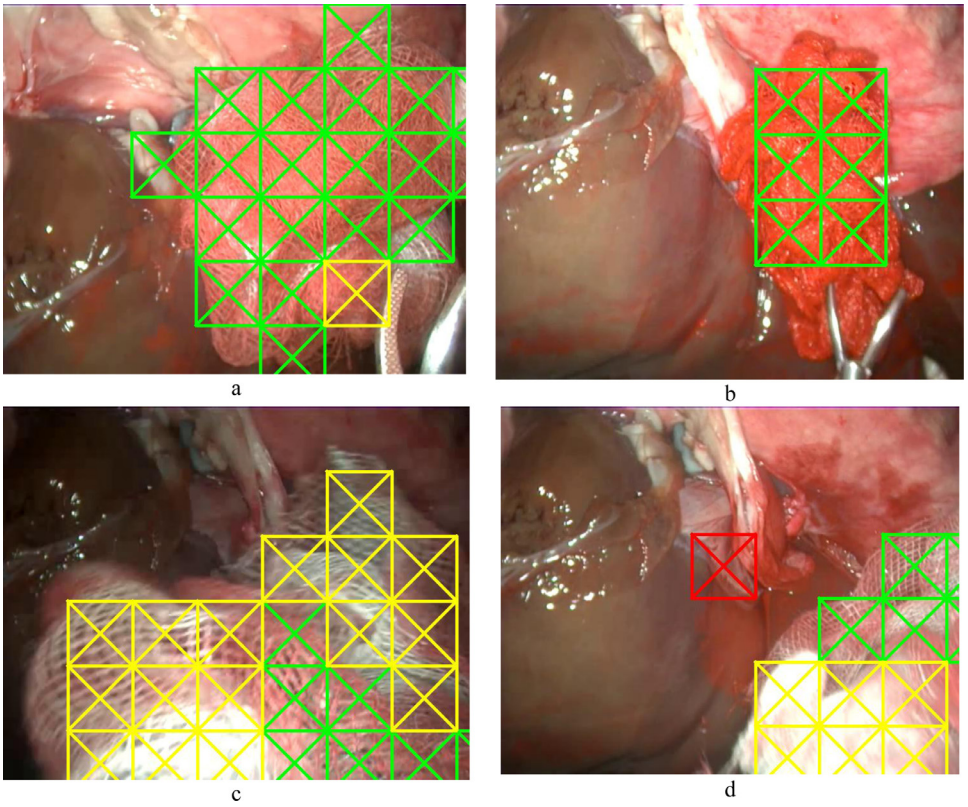

Fig. 8. CLBP Results. True positives are marked in green, false positives in red and the false negatives in yellow. The detection of CLBP on a) stained and b) soaked gauzes is nearly perfect but it fails in c) blurred and d) saturated areas of the images d) Highly textured tissues in the background can also generate false positives (in red). (Link to all the CLBP results on the test suite).

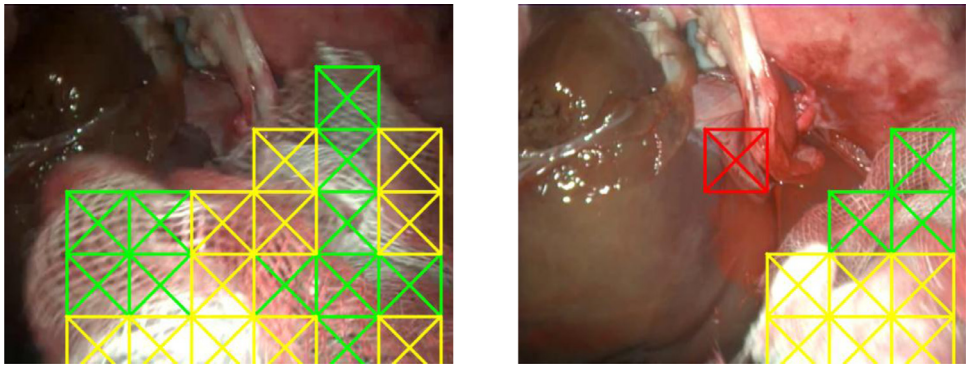

Fig. 9. ResNet50 provides better results on any type of image but it also fails in blurred images and saturated areas. (Link to all the results using ResNet50 on the test suite).

Table 4
Precision and sensitivity obtained by the CLBP algorithm. (More detailed table in the following link.).

CLBP		
Image content	precision	sensitivity
Clean gauze	1.0	0.91
Stained gauze	0.98	0.88
Soaked gauze	0.90	0.87
Overall	**0.98**	**0.89**

Table 5
Precision and sensitivity obtained by the ResNet50 CNN. (More detailed table in this link).

CNN ResNet50		
Image content	precision	sensitivity
Clean gauze	1.0	0.98
Stained gauze	1.0	0.93
Soaked gauze	0.98	0.99
Overall	**1.00**	**0.97**

4.3. ResNet50 CNN

LBP methods are computationally efficient and present robustness to rotation of the gauze pattern. They are even resilient to variations in scene illumination, as long as these are not excessive. Unfortunately, there are other disturbances in the image acquisition conditions that have to be faced when working with an endoscope in a surgical operation such as strong changes in the point of view that significantly vary the spatial scale of the pattern, image blurring due to movement of the endoscope and saturation of gauze white areas in the image. All these uncontrolled imaging conditions are difficult to model in the design of a priori hand-crafted descriptors such as the ones we have presented.

The ResNet50 convolutional neural network has been trained to classify between gauze or background and its performance has been tested on 110 images of a different dataset. The results provided by this off-the-shelf neural network (see Table 5) exceed in precision and sensitivity those obtained by our previous hand crafted LBP texture algorithms. This confirms the remarkable performance of the neural approach in this type of problems where the image acquisition conditions are variable. However, the neural network is also incapable to detect the gauze in situations of saturation and blurring and produces false positives in highly textured background tissues (Fig. 9). In this case, the results probably would have been better using a data set containing a wide range of images in order that the neural network learns from a variety of different patterns. The problem of training on a very large data set could be overcome by combining convolutional networks with the handcrafted LBP descriptors producing a high performing system that exceeds CNN trained specifically on a given dataset [24].

Table 6
Final precision and sensitivity obtained by the gauze detection algorithm after connected components analysis.

	LBP|VAR		CLBP	
Image content	Precision	Sensitivity	Precision	Sensitivity
Clean gauze	1.0	0.93	1	0,96
Stained gauze	0.96	0.94	0,98	0,95
Soaked gauze	0.90	0.92	0,94	0,94
Overall	**0.96**	**0.93**	**0.98**	**0.94**

4.4. Connected components analysis

In this subsection we present a simple and efficient morphological post-processing that mitigates some detection deficiencies that appears in saturated image areas or in highly textured background tissues.

Saturated image areas are usually surrounded by other blocks where gauze has been found. A mathematical morphology closing operation with a 3×3 structuring element can partially correct the lack of detection. Similarly, false positives originated by tissues with a lot of texture produce usually small connected components with only a few blocks. In this case, a size filter on the connected components can eliminate these erroneous blobs integrated by only a few blocks.

We have applied this simple post-processing chain to the results obtained by the LBP|VAR and the CLBP algorithm. The improvement is substantial in both cases (links to the image results using this post-processing on LBP|VAR and CLBP classification). The results obtained show that this morphological post-processing increases the detection sensitivity in any type of image without degrading the precision. The detection for LBP|VAR and CLBP methods reaches an overall sensitivity of 93% and 94% respectively. Table 6 details the sensitivity and precision obtained in the different types of images (more detailed tables in LBP|VAR final table and CLBP final table).

Table 7 presents several hyperlinks to video results. The videos, with different contents, have all been processed with the proposed parameters: 100×100 pixel blocks, neighborhood size P=8, and radius R=1.

4.5. Execution time

Execution time is an important factor in this practical computer vision application because it is necessary to process the video in real time. The LBP algorithms has been coded in C++ using the

Table 7
Results obtained on videos with different contents.

Video Results			
Video contents	LBP	LBP|VAR	CLBP
Clean gauze	video	video	video
Stained gauze	video	video	video
Soaked gauze	video	video	video

OpenCV library [27] (link to code). The average execution time for the LBP|VAR variant, including the morphological postprocessing, in the suite of 720 × 576 test images is 15 milliseconds in a 4-core Intel Core i7-4720HQ 2.6GHz. This execution speed allows the video processing at 50 fps without problem. As long as CLBP algorithm is concerned, it needs 13 milliseconds on average on the same computer. In the case of higher resolution video processing, speed can be further improved because both algorithms are easily parallelized on a normal multicore processor [6].

However, the average processing time for each image using the neural network is 4,22 seconds. Although this time cannot be directly compared with those obtained in LBP methods because it has been executed in another machine and under different programming language, this processing time is much higher (x300) than for LBP operators. This time can be drastically improved by running the CNN on a GPU and rewriting some parts in C++ or CUDA but accelerating the execution 300 times seems difficult using a regular computer.

5. Conclusions

Several technologies have been developed in recent years to avoid the inadvertent retention of surgical gauzes, but this medical error is still a major problem. The proposed solution presents several advantages over other existing equipment as it works autonomously and transparently for the surgeon, making the process of monitoring these items more direct and convenient. The presented video processing application is also cost-effective since it does not require, apart from the endoscope, the acquisition of new devices or specialized hardware and it can be used in conjunction with other technologies to make gauze control absolutely reliable.

We have proposed two LBP algorithms that have proven to be reliable for the detection and monitoring of the gauze under the different appearances that it may show in laparoscopic surgery. The results obtained are promising, with final precision of 96% and sensitivity of 93% for LBP|VAR and precision of 98% and sensitivity of 94% for CLBP. Although the latter variant has better performance percentages, the former has been revealed to be more robust to image blurring, a situation commonly encountered in laparoscopy due to the frequent movement of the endoscope and gauze. Both methods present a simple and efficient computational implementation, which is mandatory for high-definition video processing in real time.

Future lines of improvement will necessarily include CNN networks. In this paper we have also explored this approach with a ResNet50 neural network and the results obtained, with a precision of 100% and sensitivity of 97%, exceed those provided by our hand crafted LBP texture algorithms. This confirms the remarkable performance of the neural approach in this type of problems where the image acquisition conditions are variable. However, CNN practical implementation in a normal computer is currently hampered by its excessive computational cost.

Declaration of Competing Interest

The authors declare that they have no conflict of interest.

Acknowledgements

This work has been funded by the Spanish Ministry of Economy, Industry and Competitiveness, through the project DPI2016-80391-C3-3-R.

Supplementary materials

Supplementary material associated with this article can be found, in the online version, at doi:10.1016/j.cmpb.2020.105378.

References

[1] R. Bello-Cerezo, F. Bianconi, F. Di Maria, P. Napoletano, F. Smeraldi, Comparative evaluation of hand-crafted image descriptors vs. Off-the-Shelf CNN-Based features for colour texture classification under ideal and realistic conditions, Appl. Sci. 9 (4) (2019) 738 (Switzerland)art. no..
[2] S. Banerji, A. Verma, C. Liu, LBP and color descriptors for image classification, Cross Disciplinary Biometric Systems. Intelligent Systems Reference Library, 37, Springer, 2012.
[3] Canziani A., Paszke A., Culurciello E.An analysis of deep neural network models for practical applications. 24 de mayo de2016(accesed 15 november 2019); Available in:http://arxiv.org/abs/1605.07678
[4] R.R. Cima, A. Kollengode, J. Garnatz, A. Storsveen, C. Weisbrod, C. Deschamps, Incidence and characteristics of potential and actual retained foreign object events in surgical patients, J Am. Coll Surg 207 (1) (2008) 80–87, doi:10.1016/j.jamcollsurg.2007.12.047.
[5] L. Chen, W. Tang, N.W. John, T. Wan, J.J. Zhang, SLAM-based dense surface reconstruction in monocular minimally invasive surgery and its application to augmented reality, in: Computer Methods and Programs in Biomedicine, 158, Elsevier, 2018, pp. 135–146.
[6] E. de la Fuente, F.M. Trespaderne, L. Santos, J.C. Fraile, J.P. Turiel, Parallel computing for real time gauze detection in laparoscopy images, in: 2017 2nd International Conference on Bio-engineering for Smart Technologies (BioSMART), Paris, 2017, pp. 1–5, doi:10.1109/BIOSMART.2017.8095328.
[7] A. García-Martínez, C.G. Juan, N.M. Garcia, J.M. Sabater-Navarro, Automatic detection of surgicalgsing computer vision, 2015 23rd Mediterranean Conference on Control and Automation (MED), 2015 June 16-19.
[8] A.A. Gawande, D.M. Studdert, E.J. Orav, T.A. Brennan, M.J. Zinner, Risk factors for retained instruments and sponges after surgery, N. Engl. J. Med. 348 (3) (2003) 229–235.
[9] C.C. Greenberg, R. Diaz-Flores, S.R. Lipsitz, S.E. Regenbogen, L. Mulholland, F. Mearn, S. Rao, T. Toidze, A.A. Gawande, Bar-coding surgical sponges to improve safety: a randomized controlled trial, Ann. Surg. 247 (2008) 612–616 (April (4)), doi:10.1097/sla.0b013e3181656cd5.
[10] Z. Guo, L. Zhang, D. Zhang, Rotation invariant texture classification using LBP variance (LBPV) with global matching, Pattern Recognit. 43 (2010) 706–719, doi:10.1016/j.patcog.2009.08.017.
[11] Z. Guo, L. Zhang, D. Zhang, A completed modeling of local binary pattern operator for texture classification IEEE Trans, Image Process 19 (6) (2010) 1657–1663.
[12] D. Hariharan, D.N. Lobo, Retained surgical sponges, needles and instruments, Ann. R. Coll. Surg. Engl. 95 (2) (2013) 87–92, doi:10.1308/003588413X13511609957218.
[13] K. He, X. Zhang, S. Ren, J. Sun, Deep residual learning for image recognition, in: 2016 IEEE Conference on Computer Vision and Pattern Recognition (CVPR), Las Vegas, NV, IEEE, 2016, pp. 770–778.
[14] M. Heikkilä, M. Pietikäinen, C. Schmid, Description of interest regions with center-symmetric local binary patterns, in: Proceedings of 5th Indian Conference of Computer Vision, Graphics and Image Processing, 2006, pp. 58–69.
[15] A. Lazzaro, A. Corona, L. Iezzi, S. Quaresima, L. Armisi, I. Piccolo, C.M. Medaglia, S. Sbrenni, P. Sileri, N. Rosato, A.L. Gaspari, N. Di Lorenzo, Radiofrequency-based identification medical device: an evaluable solution for surgical sponge retrieval? Surg. Innovat. 24 (3) (February 2017) 155335061769060, doi:10.1177/1553350617690608.
[16] L. Liu, P. Fieguth, Y. Guo, X. Wang, M. Pietikäinen, Local binary features for texture classification: taxonomy and experimental study, Pattern Recognit. 62 (2017) 135–160.
[17] L. Liu, J. Chen, G. Zhao, P. Fieguth, X. Chen, M. Pietikainen, Texture classification in extreme scale variations using GANet, IEEE Trans. Image Process. 28 (8) (2019) 3910–3922 art. no. 8663448.
[18] A.E. Lincourt, A. Harrell, J. Cristiano, C. Sechrist, K. Kercher, B.T. Heniford, Retained foreign bodies after surgery, J. Surg. Res. 138 (2) (2007) 170–174, doi:10.1016/j.jss.2006.08.001.
[19] C. López-Casado, E. Bauzano, I. Rivas-Blanco, V.F. Muñoz, J.C. Fraile, Collaborative robotic system for hand-assisted laparoscopic surgery, in: A. Ollero, A. Sanfeliu, L. Montano, N. Lau, C. Cardeira (Eds.), ROBOT 2017: Third Iberian Robotics Conference. ROBOT 2017, 694, Advances in Intelligent Systems and Computing, 2018.
[20] T. Mäenpää, T. Ojala, M. Pietikäinen, M. Soriano, "Robust texture classification by subsets of local binary patterns, in: Proc. 15th International Conference on Pattern Recognition, 3, 2000, pp. 947–950.

[21] T. Mäenpää, M. Pietikäinen, Texture analysis with local binary patterns, in: C.H. Chen, P.S.P. Wang (Eds.), Handbook of Pattern Recognition and Computer Vision, eds.3rd edn., World Scientific, Singapore, 2005, pp. 197–216.
[22] L. Maier-Hein, P. Mountney, A. Bartoli, H. Elhawary, D. Elson, A. Groch, A. Kolb, M. Rodrigues, J. Sorger, S. Speidel, D. Stoyanov, Optical techniques for 3D surface reconstruction in computer-assisted laparoscopic surgery, in: Medical Image Analysis, 17, Elsevier, 2013, pp. 974–996.
[23] A. Muñoz-García, E. de la Fuente-López, L. Santos del Blanco, J.C. Fraile-Marinero, J. Pérez-Turiel, Sistema de Visión para Seguimiento Automático de Gasas Quirúrgicas en Cirugía Laparoscópica, Actas de las XXXIX Jornadas de Automática (2018) 72–79 Badajoz (Spain), 5-7 de Septiembre de http://dehesa.unex.es/bitstream/handle/10662/8134/978-84-09-04460-3_072.pdf?sequence=1&isAllowed=y .
[24] Nanni, L., Ghidoni, S., Brahnamb, S.Ensemble of convolutional neural networks for bioimage classification. Appl. Comput. Informat.https://doi.org/10.1016/j.aci.2018.06.002
[25] T. Ojala, M. Pietikäinen, D. Harwood, "A comparative study of texture measures with classification based on feature distributions, Pattern Recognit. 29 (1) (1996) 51–59.
[26] T. Ojala, M. Pietikäinen, T. Mäenpää, Multiresolution gray-scale and rotation invariant texture classification with local binary patterns, IEEE Trans. Pattern Anal. Mach. Intell. 24 (7) (2002) 971–987.
[27] OpenCV Library. Available from: http://opencv.org/ (acc. June 11, 2019).
[28] M. Pietikäinen, T. Ojala, Z. Xu, Rotation-invariant texture classification using feature distributions, Pattern Recog. 33 (2000) 43–52.
[29] M. Pietikäinen, T. Mäenpää, J. Viertola, Color texture classification with color histograms and local binary patterns, in: Workshop on Texture Analysis in Machine Vision, 2002, pp. 109–112.
[30] M. Pietikäinen, G. Zhao, A. Hadid, T. Ahonen, Computer vision using local binary patterns, Number 40 in Computational Imaging and Vision, Springer, 2011.
[31] M.E. Rabie, M.H. Hosni, A. Al Safty, M. Al Jarallah, F.H. Ghaleb, Gossypiboma revisited: a never ending issue, Int. J. Surg. Case Rep. 19 (2016) 87–91, doi:10.1016/j.ijscr.2015.12.032.
[32] A. Rehman, N. Ul-Ain Baloch, M. Awais, Gossypiboma (Retained Surgical Sponge): an evidence-based review, Open J. Surg 1 (1) (2017) 008–014.
[33] G. Schaefer, N. Doshi, LBP vs. LBP variance for texture classification, in: Y. Tan, H. Takagi, Y. Shi (Eds.), Data Mining and Big Data. DMBD 2017. Lecture Notes in Computer Science, 10387, Springer, Cham, 2017.
[34] V.M. Steelman, M.H. Alasagheirin, Assessment of radiofrequency device sensitivity for the detection of retained surgical sponges in patients with morbid obesity, Arch. Surg. 147 (2012) 955–960.
[35] V.M. Steelman, J.J. Cullen, Designing a safer process to prevent retained surgical sponges: a healthcare failure mode and effect analysis, AORN J 94 (2) (2011) 132–141.
[36] V.M. Steelman, C. Shaw, L. Shine, A.J. Hardy-Fairbanks, Retained surgical sponges: a descriptive study of 319 occurrences and contributing factors from 2012 to 2017, Patient Saf. Surg. 12 (2018) 20 Published 2018 Jun 29., doi:10.1186/s13037-018-0166-0.
[37] Storz. Karl Storz Endoskopes. https://www.karlstorz.com/es/es/telepresence.htm
[38] X. Tan, B. Triggs, Enhanced local texture feature sets for face recognition under difficult lighting conditions, IEEE Trans. Image Process. 19 (6) (2010) 1635–1650.
[39] Y. Zhao, D.S. Huang, W. Jia, Completed local binary count for rotation invariant texture classification, IEEE Trans. Image Process. 21 (10) (2012) 4492–4497.